STEM CELLS TRANSLATIONAL MEDICINE®

ENABLING TECHNOLOGIES FOR CELL-BASED CLINICAL TRANSLATION

Bone Marrow Regeneration Promoted by Biophysically Sorted Osteoprogenitors From Mesenchymal Stromal Cells

ZHIYONG POON,[a] WONG CHENG LEE,[a,b] GUOFENG GUAN,[a,c] LIN MYINT NYAN,[a] CHWEE TECK LIM,[a,b,c,d,e] JONGYOON HAN,[a,f,g] KRYSTYN J. VAN VLIET[a,g]

Key Words. Tissue regeneration • Adult stem cells • Bone marrow • Mesenchymal stem cells

[a]BioSystems & Micromechanics IRG, Singapore-MIT Alliance in Research and Technology, Singapore; [b]Graduate School for Integrative Sciences and Engineering, [d]Department of Biomedical Engineering, and [c]Department of Mechanical Engineering, National University of Singapore, Singapore; [e]Mechanobiology Institute, Singapore; [f]Department of Electrical Engineering and Computer Science and [g]MIT Biological Engineering, Massachusetts Institute of Technology, Cambridge, Massachusetts, USA

Correspondence: Krystyn J. Van Vliet, Ph.D., 77 Massachusetts Avenue, Room 8-237, Cambridge, Massachusetts 02139, USA. Telephone: 617-253-3315; E-Mail: krystyn@mit.edu

Received August 3, 2014; accepted for publication October 1, 2014; first published online in SCTM *Express* November 19, 2014.

1066-5099/2014/$20.00/0

http://dx.doi.org/10.5966/sctm.2014-0154

ABSTRACT

Human tissue repair deficiencies can be supplemented through strategies to isolate, expand in vitro, and reimplant regenerative cells that supplant damaged cells or stimulate endogenous repair mechanisms. Bone marrow-derived mesenchymal stromal cells (MSCs), a subset of which is described as mesenchymal stem cells, are leading candidates for cell-mediated bone repair and wound healing, with hundreds of ongoing clinical trials worldwide. An outstanding key challenge for successful clinical translation of MSCs is the capacity to produce large quantities of cells in vitro with uniform and relevant therapeutic properties. By leveraging biophysical traits of MSC subpopulations and label-free microfluidic cell sorting, we hypothesized and experimentally verified that MSCs of large diameter within expanded MSC cultures were osteoprogenitors that exhibited significantly greater efficacy over other MSC subpopulations in bone marrow repair. Systemic administration of osteoprogenitor MSCs significantly improved survival rates (>80%) as compared with other MSC subpopulations (0%) for preclinical murine bone marrow injury models. Osteoprogenitor MSCs also exerted potent therapeutic effects as "cell factories" that secreted high levels of regenerative factors such as interleukin-6 (IL-6), interleukin-8 (IL-8), vascular endothelial growth factor A, bone morphogenetic protein 2, epidermal growth factor, fibroblast growth factor 1, and angiopoietin-1; this resulted in increased cell proliferation, vessel formation, and reduced apoptosis in bone marrow. This MSC subpopulation mediated rescue of damaged marrow tissue via restoration of the hematopoiesis-supporting stroma, as well as subsequent hematopoiesis. Together, the capabilities described herein for label-freeisolation of regenerative osteoprogenitor MSCs can markedly improve the efficacy of MSC-based therapies.
STEM CELLS TRANSLATIONAL MEDICINE *2015;4:56–65*

INTRODUCTION

Since the discovery and demonstration of multilineage differentiation potential, bone marrow (BM)-derived mesenchymal stromal cells (MSCs) have generated considerable interest as candidates for cell-based tissue regenerative therapies, with the implicit idea that they function primarily as self-renewing stem cells that replace damaged tissue [1, 2]. However, retrospective clinical and laboratory investigations have indicated another possible role for MSCs as regenerative "cell factories" that secrete beneficial factors capable of facilitating tissue recovery on many potential levels. Those mechanisms include the stimulation of endogenous stem/progenitor cells, cell proliferation, and angiogenesis, as well as the suppression of inflammation and cell death [3]. This paracrine signaling function of MSCs has now been substantiated in several hallmark studies of emerging medical applications for MSCs in areas of wound healing, as well as neurological, cardiac, and vessel regeneration: therapeutic improvement was attributed chiefly to the presence of a regenerative secretome rather than to significant direct engraftment and differentiation of MSCs into cells comprising the injured tissue [3–7].

Strategically, this shift in focus to the role of MSCs as cell factories has important consequences for clinical translation of cell-based regenerative therapies. Part of this shift reflects greater appreciation that MSC populations are heterogeneous, particularly when culture-expanded to large numbers in vitro, and include a subset of mesenchymal stem cells that exhibit in vitro self-renewal capacity or multilineage differentiation [8, 9]. First is the implication that MSC potency may also vary significantly with the tissue or microenvironment of origin [10]. Several studies have established that MSCs derived from adipose tissue, umbilical cord, and BM have different gene expression profiles, although MSCs from each source can exhibit multipotent differentiation [11, 12]. The secretome of these MSCs could therefore vary greatly depending on the biologic relationship between the MSC and its tissue of

origin and should be verified preclinically before therapeutic use. Second, and related to the preceding point, is the possibility that relevant therapeutic factors may be present or enhanced in the secretome from only the lineage-committed progenies of the mesenchymal stem cells. It is plausible that those progenitor cell subpopulations could thus be more therapeutically efficacious than uncommitted, multipotent MSCs (i.e., stem cells) for some translational applications. Recent investigations of the physiological roles of MSCs and their progenitors within the marrow have provided insight into their different possible therapeutic values [5, 13–17]. Literature observations have alluded to a connection between BM-derived MSCs with high osteogenic activity and the capabilities for microenvironmental repair as well as HSC support, both of which critical for BM homeostasis. For example, genetic pulse-chase experiments have indicated that osteoprogenitors responsible for repairing bone tissue injury are transient, nonproliferative cells that require replenishment from a pool of uncommitted MSCs precursors [18]. Similarly, other studies investigating the effects of irradiation or similar myeloablative procedures demonstrate that during BM recovery, the surviving perivascular MSCs proliferate and undergo a reversible and transient shift toward a state of higher osteogenic activity [19–22]. This was indicated by an increased expression of osteoblastic differentiation markers such as alkaline phosphatase, osteopontin, osteocalcin, and Runx2 (runt-related transcription factor 2) during the recovery period [23].

The means to produce therapeutically relevant numbers of MSCs that are manipulated toward an osteoprogenitor state could therefore have significant impact for applications in BM or hematopoietic regeneration. Osteoblasts or preosteoblasts cannot be isolated easily from BM aspirates, because cells adhere strongly to mineralized matrix and require enzymatic treatment for extraction [24]. MSCs in typical bone marrow aspirates are predominantly from the perivascular BM space [13]. In vivo, these MSCs can give rise to osteoprogenitors and eventually the osteoblasts that mineralize bone. This capability for osteogenic commitment is retained ex vivo but can also occur in an uncontrolled and stochastic manner during basal (noninductive) culture expansion [25]. Immunophenotyping approaches for identifying osteoprogenitor MSCs such that they can be purified from the larger population of culture-expanded cells for therapeutic applications is a possible strategy, but this approach is inefficient and limited by a lack of sufficiently specific markers. Further, those surface markers that are expressed by MSCs constitutively are not useful indicators of the osteogenic lineage commitment process [8, 26, 27]. We have previously characterized biophysically distinct subpopulations in culture-expanded MSCs and identified several physical properties that are predictive of the phenotype, expression profiles, and differentiation potency in vitro and in vivo [28]. Those subpopulations were indistinguishable via typical "mesenchymal stem cell" surface antigens quantified via flow cytometry. However, from such a heterogeneous, culture-expanded MSC population, an osteoprogenitor subpopulation can be conveniently distinguished from other MSC subpopulations by a larger cell diameter $>$ approximately 20 μm, concurrent with higher cell stiffness and lower degree of nuclear membrane fluctuations.

Herein, to translate these findings to clinical relevance, we used a high-throughput, biophysical, and label-free microfluidic sorting approach to isolate the osteoprogenitor MSCs from the culture-expanded BM-derived MSC population for subsequent evaluation of regenerative capabilities in a BM injury model. We found that osteoprogenitor MSCs are potent cell factories that can mediate rapid regeneration of myeloablated BM, which fosters an environment conducive to hematopoietic recovery. Although this work primarily investigates the use of these cells for BM tissue repair, other medical indications could also potentially benefit from use of these biophysically sorted cells. Further, this inertial microfluidic-based approach represents a significant advantage over current antibody- or fluorescence-based strategies to identify and select for MSC subpopulations. Not only is it readily amenable to scale-up, this biophysical sorting also does not require the use of additional biologics in the isolation process (as in fluorescence-activated cell sorting [FACS] or cell separation columns), thus mitigating the risk of augmented MSC properties or contamination for human clinical use.

Materials and Methods

Materials and Methods are included in the supplemental online data.

Results

Label-Free Microfluidic Enrichment of MSC Osteoprogenitors

Initial MSC populations were obtained commercially from adult human BM aspirates via Ficoll density centrifugation and tissue culture plastic adherence; this process is designated as the first passage (P). These culture-expanded populations are often referred to collectively as mesenchymal stem cells, and here we note their heterogeneity by referring to this population as mesenchymal stromal cells. MSCs were culture-expanded using conventional protocols (see Materials and Methods in the supplemental online data) over a maximum of 9 passages or over 20 population doublings. At P2, MSCs were uniform in morphology and size; MSCs also expressed surface markers CD44, CD73, CD90, CD105, CD140B, CD146, and CD166 but not CD19, CD45, CD106, Nestin, Stro-1, or NG2 (supplemental online Fig. 1).

To separate the osteoprogenitors from other MSCs, we used an inertial microfluidic device with a single inlet and two outlets; the microfluidic spiral channel exhibited a trapezoidal cross-section of 80-μm inner depth, 130-μm outer depth, and 600-μm channel width (Fig. 1A) [29, 30]. This design enabled separation of larger from smaller cells in the fluid suspension at high throughput rates of up to 3 million cells per minute at high viability postsorting ($>$95%). Such size-based fractionation of suspended cells leveraged previous findings that larger MSCs also exhibited characteristics of committed osteoprogenitors in vitro and in vivo [28, 31]. This approach focused cells with larger diameter toward the inner channel region and directed smaller cells into the Dean vortices at the outer channel region (Fig. 1B). Optimal processing rates for size-based cell separation of 3.0 ml/minute were identified through initial sorting of polystyrene beads as reported previously [30]. High-speed imaging of the MSC sorting process at the channel bifurcation showed the larger and smaller MSCs diverging toward the inner and outer outlets, respectively (Fig. 1Ci). The collected MSC subpopulations were distinctly different in size, as shown in Figure 1Cii and 1Ciii. This resulted in two MSC subpopulations (Fig. 1D): one highly enriched in cells of larger mean diameter D ($D^{hi} \approx 20\ \mu$m) and one depleted in those larger cells and thus characterized by a lower mean cell diameter ($D^{lo} \approx 15\ \mu$m). Optical imaging of adherent cells confirmed that a significantly greater number of large, flat, and

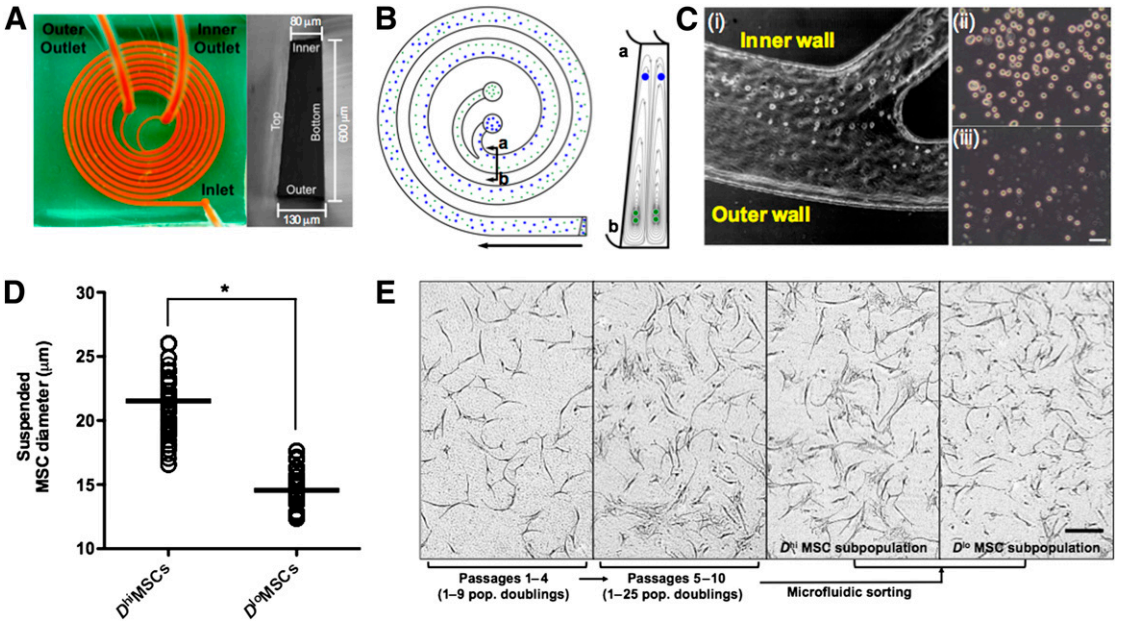

Figure 1. Enrichment of osteoprogenitor MSCs using a label-free, microfluidic sorting approach. **(A):** Spiral microfluidic sorter. Suspended MSCs are injected at the inlet, and two cell subpopulations of differing diameter *D* are obtained at the inner and outer outlet, respectively. **(B):** Schematic of and working principle of device in **(A)**. During their path through the spiral sorter, particles can be separated based on inertia, with particles of larger diameter accumulating near the inner channel and smaller particles deflected toward the outer channel. **(C):** High speed images of MSC sorting process at the outlets **(Ci)**, with the D^{hi} and D^{lo} MSCs sorted toward the inner and outer channel walls, respectively. The resultant sorted D^{hi} and D^{lo} MSC subpopulations collected at the inner and outer outlet are shown in **(Cii)** and **(Ciii)**, respectively. Scale bar = 50 μm. **(D):** The size distribution of sorted MSCs (passage 6 [P6], $n > 500$ cells counted from each of 4 donors) are: D^{hi} MSCs = 21.9 $\pm$ 5.3 μm, D^{lo} MSCs = 14.8 $\pm$ 2.4 μm. $*$, $p = .0002$. Data given as means $\pm$ SEM. **(E):** During in vitro culture, early passage MSCs are uniform in morphology and size, but a larger and flatter MSC subpopulation is evident after ~10 population doublings. The resultant expanded MSC culture is heterogeneous in size and morphology. The microfluidic sorter in **(A)** was used for size sorting of expanded MSCs into D^{hi} and D^{lo} MSC subpopulations. These MSC subpopulations differed morphologically after plating on tissue culture plastic. Compared with unsorted MSCs (P6), the subpopulation of larger and flatter MSCs was enriched by more than fivefold in the sorted D^{hi} MSC subpopulation. Scale bar = 100 μm. Abbreviations: MSC, mesenchymal stromal cell; pop., population.

irregularly shaped cells were present in the D^{hi} MSC subpopulation but not in the D^{lo} MSC subpopulation (Fig. 1E).

As described previously, we observed an increasing number of larger and flatter cells within the adherent, culture-expanded populations over increasing passages; this subpopulation comprised 20%–30% of the MSC population by P5–P6 (Fig. 1E) [31]. Extensive device testing with MSCs derived from BM of seven different adult donors showed that the sorted fractions across P5–P7 were consistent in cell diameter (D^{hi} MSCs = 21.9 $\pm$ 5.3 μm, D^{lo} MSCs = 14.8 $\pm$ 2.4 μm; Fig. 1D). Unless otherwise noted, the results below were obtained for MSCs sorted at P6, which generated a more than fivefold enrichment of D^{hi} MSCs as compared with the unsorted MSC population. These D^{hi} MSC subpopulations exhibited minimal proliferative capabilities and maintained this cell size even after two additional passages (supplemental online Fig. 3A, 3B). These findings of increased prevalence and reduced proliferation of D^{hi} MSCs upon passaging are corroborated by long-term tracking experiments reported by Whitfield et al. [31] on (unsorted) MSC cultures; those studies demonstrated D^{hi} MSCs to be generated from smaller MSCs upon cell cycle exit that accumulate in population fraction with increased passaging.

D^{hi} MSC Subpopulations Exhibit Properties of Lineage-Restricted Osteoprogenitors

The osteoprogenic character of the D^{hi} MSC subpopulations thus sorted was established from genetic and functional assays. First, reverse transcription-polymerase chain reaction analysis showed increased expression of early osteogenic transcripts (osteopontin and Runx2) by D^{hi} MSCs as compared with D^{lo} MSCs but no detectable differences in late osteogenic (osteocalcin), adipogenic (peroxisome proliferator-activated receptor γ [Pparγ]), or chondrogenic (Sox9) transcript expression (Fig. 2A). Antibody staining detected a significant level of osteopontin only in the D^{hi} MSC subpopulation, and osteocalcin was not detected in either MSC group (Fig. 2B). In vitro trilineage differentiation assays comparing multipotency of these size-sorted MSC subpopulations also demonstrated functional differences. D^{hi} MSC-enriched subpopulations exhibited more than threefold greater mineralization indicative of osteogenic potential, but almost sixfold less oil droplet formation indicative of adipogenic potential; chondrogenic differentiation potential was indistinguishable between these MSC subpopulations (Fig. 2C; supplemental online Fig. 2B). Under osteogenic induction, we also observed an increased *rate* of mineralization of the D^{hi} MSC group (Fig. 2D; supplemental online Fig. 2C). Additionally, D^{hi} MSC subpopulations exhibited significantly higher levels of ALP activity even in basal (noninduction) medium, which could account for the higher rates of osteogenic differentiation (supplemental online Fig. 2C) in this sorted subpopulation. Finally, D^{hi} MSCs seeded within osteoinductive scaffolds produced a greater extent of bone mineralization for murine models in vivo (twofold greater fluorescent bisphosphonate staining; Fig. 2E, 2F), as compared with those seeded with the D^{lo} MSCs.

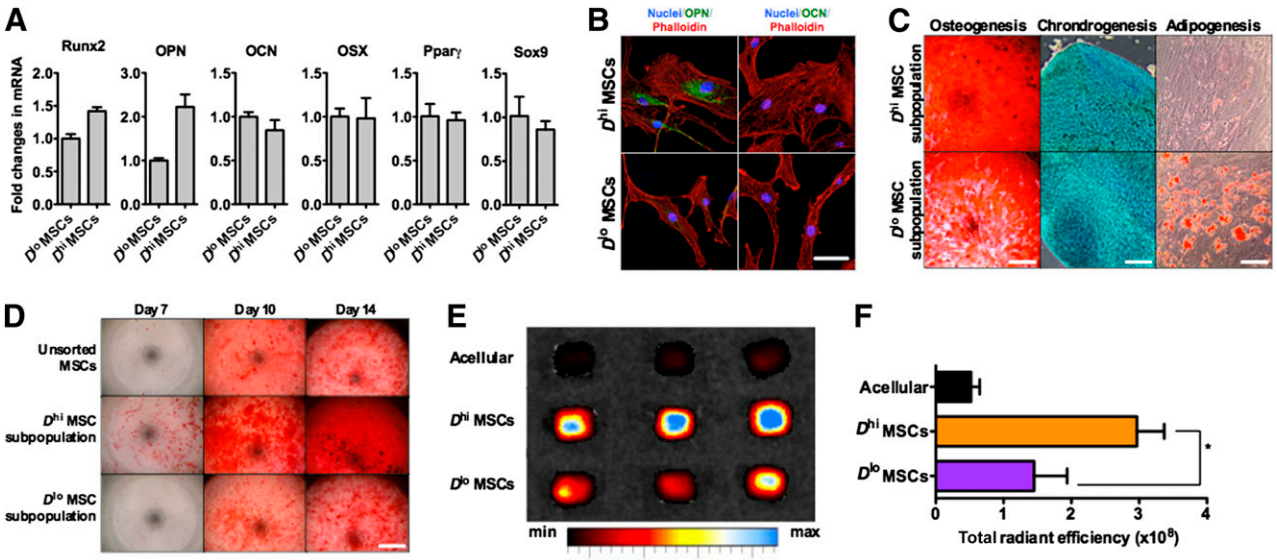

Figure 2. Characterization of microfluidic-sorted MSC subpopulations. **(A):** Representative set of data for reverse transcription-polymerase chain reaction analysis of the expression of differentiation markers for osteogenesis (Runx2, OPN, OCN, and OSX), adipogenesis (Pparγ), and chondrogenesis (Sox9). These data were normalized to glyceraldehyde-3-phosphate dehydrogenase. **(B):** Immunostaining of OPN and OCN, early and late osteogenic markers, respectively, in sorted MSCs detected OPN in only D^{hi} MSCs but no OCN in any MSC groups, suggesting that D^{hi} MSCs are osteoprogenitors. Scale bar = 50 μm. **(C):** Multilineage differentiation of sorted MSCs shows high potential for osteogenic and chondrogenic differentiation but no adipogenic differentiation of the D^{hi} MSC subpopulation. Trilineage differentiation potential was observed in the D^{lo} MSC subpopulation. Osteogenic, chondrogenic, and adipogenic formation was determined by alizarin red, Alamar Blue, and Oil Red O assays, respectively (see quantification in supplemental online Fig. 2). Scale bars = 0.4 cm (osteogenic), 5 mm (chondrogenic), and 200 μm. **(D):** Representative alizarin red staining of MSCs under osteogenic induction over a 14-day period. Quantification of alizarin red staining is shown in supplemental online Fig. 2. Scale bar = 0.4 cm. **(E):** In vivo ectopic bone formation by sorted MSCs on polycaprolactone-tricalcium phosphate scaffolds after implantation in NOD/SCIDs for 4 weeks. The degree of mineralization was measured via systemic injection of a fluorescent bisphosphonate agent 16 hours before the scaffolds were harvested and imaged ex vivo. **(F):** A significantly higher level of mineral bone formation, based on bisphosphonate staining, was found in scaffolds seeded with D^{hi} MSCs versus D^{lo} MSCs. $*$, $p = .0383$. All values are given as means $\pm$ SD. The orange bar shows the D^{hi} MSC subpopulation, the purple bar shows the D^{lo} MSC subpopulation, and the dark gray bar shows the unsorted MSC population. All MSCs were used at P6. Abbreviations: max, maximum; min, minimum; MSC, mesenchymal stromal cell; OCN, osteocalcin; OPN, osteopontin; OSX, osterix; Pparγ, peroxisome proliferator-activated receptor γ; Runx2, runt-related transcription factor 2.

Although cells in the D^{hi} MSC subpopulation exhibited a greater propensity for osteogenic differentiation, they did not exhibit mineralization under basal in vitro culture conditions; in contrast, osteoblasts and MSCs under chemical osteogenic induction do exhibit such bone mineralization capacity (supplemental online Fig. 3C). Together, these observations demonstrate the increased osteogenic but diminished adipogenic potential of the D^{hi} MSC subpopulation as compared with the D^{lo} MSCs. However, this size-sorted subpopulation was not one described as fully committed osteoblasts: cells did not express late markers of osteogenic commitment (osteocalcin) or deposit minerals spontaneously in adherent culture. Thus, we refer to the D^{hi} MSC subpopulation as osteoprogenitor MSCs. In contrast, the D^{lo} MSC subpopulation was enriched in MSCs with an uncommitted phenotype and trilineage in vitro differentiation capabilities. Importantly, despite the different functional phenotypes, both D^{hi} and D^{lo} MSC sorted subpopulations exhibited a similar surface immunophenotypic profile that is also consistent with unsorted MSCs at early in vitro passages (supplemental online Fig. 1).

D^{hi} MSC Subpopulations Promote Bone Marrow Tissue Regeneration

We used a lethally irradiated (3.5 Gy) NOD/SCID murine model to evaluate the therapeutic efficacy of intravenously injected MSCs for BM recovery. At this radiation dose, BM tissue damage is significant, and defects in the hematopoietic system occur subsequently. Untreated irradiated mice (n = 7 mice) succumbed quickly to radiation damage (median survival = 10.5 days; Fig. 3A) characterized by rapid weight loss (~40%; Fig. 2C) and depletion of white blood cells (WBCs), red blood cells (RBCs), and platelets within 5–10 days after irradiation (Fig. 3B–3E). In parallel, histological analysis revealed a severe loss of BM tissue cellularity, as well as vascular structural integrity, and quantification via flow cytometry showed a high percentage of dead or apoptotic cells (>60%) with minimal cell proliferation activity (<5%) in the BM by day 10 (Fig. 4A–4C; supplemental online Fig. 4A).

In initial experiments, unsorted MSCs at passages 3, 6, and 9 (n = 7–10 mice each) were administered systemically, 24 hours after irradiation at a cell dosage of 20×10^6 cells per kg. Overall, we found modest improvements in median survival times (12, 17, and 17 days for passage 3, 6, and 9 MSCs, respectively; supplemental online Fig. 4B) and reduced weight loss in MSC-infused mice compared with untreated mice (~30% vs. ~40% loss, respectively, within 5 days; supplemental online Fig. 4C). This indicates that MSC infusions can alleviate acute ionizing-radiation lethality. Notably, 10%–20% of mice in the treatment groups injected with MSCs at higher passages (P6 and P9) showed recovery of body weight after ~10–15 days and survived beyond 50 days, whereas none of the mice infused with MSCs from early passages (P3) survived beyond day 25. These results suggest that the D^{hi} subpopulation that increases in population fraction over

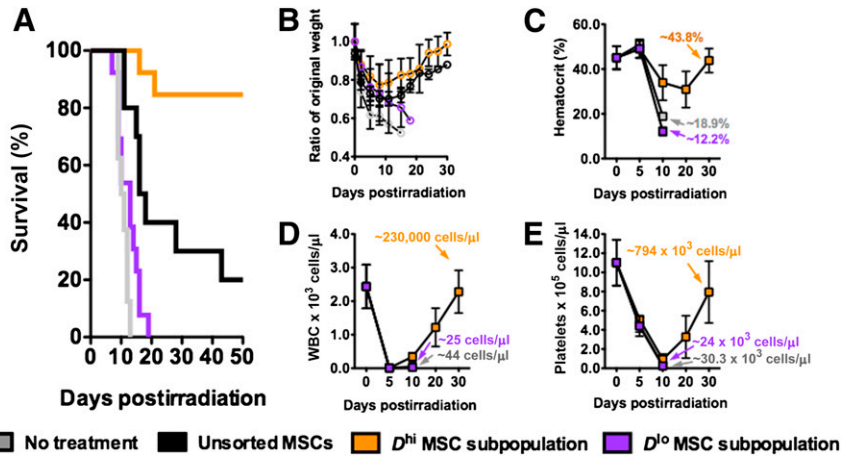

Figure 3. Bone marrow regenerative efficacies of systemically injected MSCs in lethally irradiated NOD/SCIDs (3.5 Gy). **(A):** Survival of lethally irradiated NOD/SCID mice given no treatment, unsorted MSCs, D^{hi} MSCs, and D^{lo} MSCs on day 1 after irradiation. Mean survival times were 10.5, 17, >50, and 13 days, respectively ($n > 7$ mice per group; MSC dose: 20×10^6 cells per kg). **(B):** Weight change of NOD/SCIDs in **(A)** over a period of 30 days after irradiation. **(C–E):** Whole blood counts of NOD/SCIDs for untreated D^{hi} MSC and D^{lo} MSC-injected groups. Hematopoietic recovery was detected for the D^{hi} MSC-injected group over a 30-day period. All values are given as means ± SD. The orange graphs show the D^{hi} MSC subpopulation, the purple graphs show the D^{lo} MSC subpopulation, and the dark gray graphs show the unsorted MSC population. All MSCs were used at P6. Abbreviations: MSC, mesenchymal stromal cell; WBC, white blood cell.

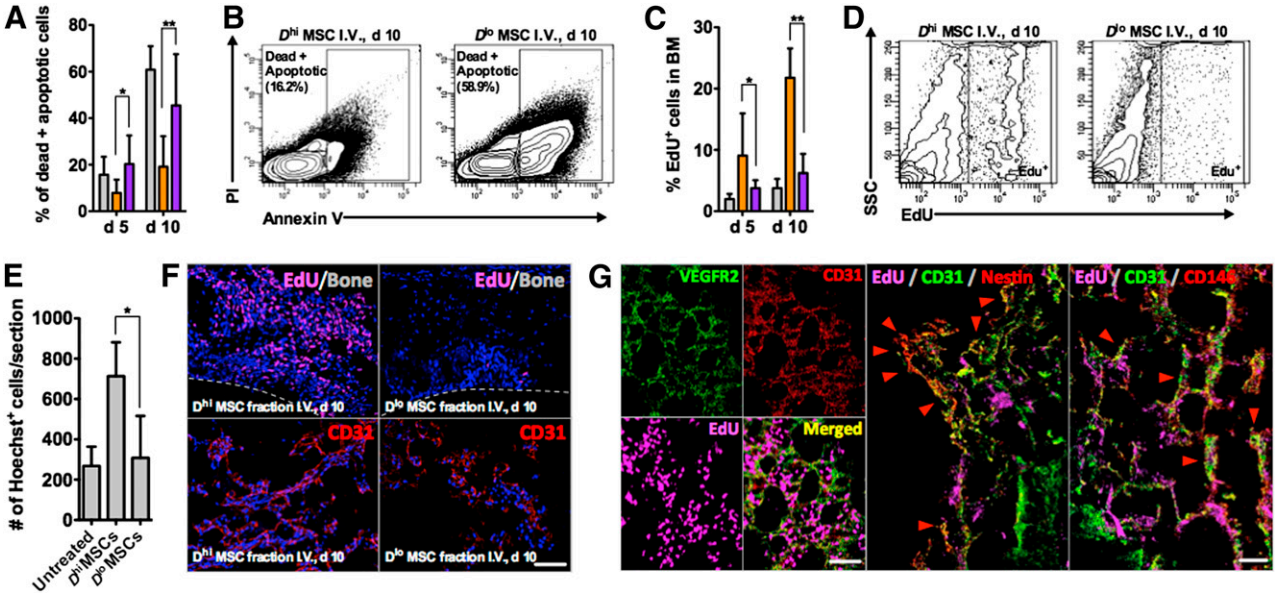

Figure 4. Analyses of the bone marrow (BM) of NOD/SCIDs in different treatment groups. **(A, B):** Fluorescence-activated cell sorting (FACS) analysis of BM aspirates at days 5 and 10, showing significantly lower numbers of dead/apoptotic cells in the BM after D^{hi} MSC injection. *, $p = .0308$; **, $p = .0231$ for days 5 and 10, respectively ($n = 8$ femoral BM aspirates tested). **(C, D):** Percentage of EdU^+ cells in the BM aspirate of different treatment groups, showing increased cell proliferation for the D^{hi} MSC-injected group. *, $p = .3263$; **, $p = .0245$ for days 5 and 10 ($n = 4$ BM aspirates tested). **(E):** Quantification of the degree of BM cellularity from histological sections. *, $p = .0378$, $n = 15$ sections analyzed from 3 different mice. **(F):** Representative histological sections of the BM after 10 days for D^{hi} and D^{lo} MSC-injected groups. BM from the D^{hi} MSC treatment group was highly cellularized and contains more EdU^+ cells and $CD31^+$ vessel structures. The dotted lines indicate the location of mineral bone. Scale bar = 100 μm. **(G):** EdU^+ cells in the D^{hi} MSC treatment group colocalized with murine CD31/VEGR2 vasculature and $nestin^+$ or $CD146^+$ stromal cells during recovery after lethal irradiation. Quantification of $nestin^+$ cell recovery is given in supplemental online Fig. 6. Scale bars = 100 μm. All values are given as means ± SD > 100,000 events are measured for FACS analysis. The orange graphs show the D^{hi} MSC subpopulation, the purple graphs show the D^{lo} MSC subpopulation, and the dark gray graphs show the unsorted MSC population. All MSCs were used at passage 6. Abbreviations: BM, bone marrow; d, day; EdU, 5-ethynyl-2′-deoxyuridine; I.V., intravenous; MSC, mesenchymal stromal cell; PI, propidium iodide; SSC, side scatter.

increased population doublings in vitro may possess properties that promote BM regeneration.

To test this hypothesis, we next evaluated the relative efficacy of osteoprogenitor-enriched D^{hi} MSC subpopulations. Compared with unsorted MSCs or the D^{lo} MSCs sorted at the same passage (P6), from the same donor, and administered at the same cell dosage, irradiated mice infused with D^{hi} MSCs exhibited dramatically improved recovery and survival (Fig. 3A, 3B). The median survival times were >50 days ($n = 13$ mice), as compared with only 17 days for unsorted MSCs ($n = 10$) and only 13 days for D^{lo} MSCs ($n = 13$).

More than 80% of the irradiated mice infused with the D^{hi} MSCs survived beyond 50 days and showed rapid recovery of body weight after ~15 days (Fig. 3B). In contrast, infusions of the D^{lo} MSCs elicited negligible impact on the recovery of lethally irradiated mice, and there were no survivors in this treatment group beyond day 20. Increased dosage of D^{lo} MSCs (to 50×10^6 cells per kg) did not improve survival (supplemental online Fig. 4D). This comparison highlights significantly distinct translational outcomes, despite no detectable difference in surface markers associated with the MSC phenotype.

Peripheral blood counts for WBCs, RBCs, and platelets dropped sharply after myeloablative irradiation. Significant decreases in hematocrit and platelet levels were observed by day 10 and corroborated with survival and weight loss. In the surviving D^{hi} MSC treatment group, endogenous hematopoietic recovery was observed after 10 days, and peripheral blood counts were restored to original levels after ~30 days (Fig. 3C–3E). Because irradiation induces significant damage and cell death in the BM, the improved survival rate of the D^{hi} MSC treatment group may plausibly be attributed to the accelerated regeneration of BM tissue with subsequent endogenous hematopoietic reconstitution. Compared with other treatment groups, FACS analysis of cells in the BM of D^{hi} MSC-treated mice showed a much lower rate of cell death (Fig. 4A, 4B; supplemental online Fig. 5A) and a higher rate of cell proliferation (Fig. 4C, 4D) over a 10-day period. Analysis of BM tissue sections obtained from these experiments further confirmed greater cellularity and 5-ethynyl-2′-deoxyuridine (EdU) incorporation after administration of D^{hi} as compared with other MSC treatment groups or untreated controls. Representative histological sections and analyses are shown in Figure 4E and 4F, as well as supplemental online Figures 4A, 5B, and 5C.

The majority of EdU^+ cells were distributed throughout the marrow and not concentrated along the mineralized regions (Fig. 4F), indicating that tissue damage and regeneration was confined to the BM vascular and extravascular compartments. When left untreated, the BM vasculature regressed significantly as a result of irradiation damage (supplemental online Fig. 5C); however, the systemic administration of D^{hi} MSCs led to the greatest extent of revascularization of the BM space by day 10 (Fig. 4F). Further examination showed colocalization of EdU with $VEGFR2^+/CD31^+$ endothelial cells of the vasculature, as well as $nestin^+$ and $CD146^+$ stromal cells in the perivascular space (Fig. 4G), indicating regeneration of the hematopoietic stem cell (HSC) vascular and perivascular niches, respectively. FACS analysis confirmed enhanced regeneration of $nestin^+$ cell populations in D^{hi} MSC treatment groups (supplemental online Fig. 6). Together, these results demonstrate the potency of D^{hi} MSC subpopulations to promote repair after BM tissue damage. This repair includes recovery of vasculature and hematopoiesis-supporting stroma cell populations after injury inflicted by irradiation, promoting recovery of irradiated mice via restoration of hematopoiesis.

MSCs Do Not Engraft Significantly Within the Bone Marrow

To determine whether MSC engraftment within injured BM enabled this therapeutic outcome, we first examined the biodistribution of intravenously injected MSCs via bioluminescence imaging of injected luciferase-transformed MSCs. No changes were found in the immunohistochemistry or trilineage differentiation capability of MSCs after transformation (supplemental online Fig. 7A, 7B). The bioluminescent signal was constitutively and equally expressed in response to injection of either D^{hi} or D^{lo} MSC subpopulations (supplemental online Fig. 7C, 7D). In vivo bioluminescence analysis of luciferase-transformed MSCs showed an approximately linear relationship between MSC number and bioluminescent signal, with a lower detection limit of 10^2–10^3 cells after subcutaneous injection (supplemental online Fig. 7E. 7F).

To observe long-term biodistribution of injected MSCs and also to provide BM injury stimulus for MSC homing, a sublethally irradiated mouse model (2.5 Gy) was used; this model demonstrated survival rates above 95% for up to 30 days even without treatment. Immediately after tail vein injection into sublethally irradiated mice, both D^{hi} or D^{lo} MSC subpopulations accumulated in the pulmonary capillary beds and gradually redistributed to the rest of the body within 24 hours (Fig. 5A; supplemental online Fig. 8A). Over this period of distribution, the MSC bioluminescent signal did not localize specifically to any organ or body part, and longer-term imaging showed no distinct differences in the overall biodistribution patterns of the size-sorted subpopulations. All bioluminescent signals were below detection limits by days 10–15. In other words, engraftment in specific organs or in the marrow was not evidenced for either subpopulation.

We additionally evaluated histological sections of lung tissue at 24 hours after MSC injection, to determine whether MSCs engrafted within the lung after tail vein injection. Human specific staining for β2-microglobulin in these lung sections showed that only a small amount of injected MSCs extravasated into lung tissue (Fig. 5B) and that no MSCs were found in the lungs after 2 weeks. This finding corroborated bioluminescent tracking observations. FACS examination of whole BM aspirates further showed that, regardless of MSC passage or sorted subpopulation, only a small number of human MSCs (typically between 0.02% and 0.20% of the injected dose and less than 5% of total BM cells analyzed) homed to the BM by day 5. Those MSCs that did localize to the BM were further diminished after day 10 (Fig. 5C; supplemental online Fig. 8B, 8C). Longer-term studies of the lungs, liver, BM, and spleen 30 days after injection showed less than 0.001% of injected human MSCs remained in the host tissue. Therefore, the short residence times and low accumulation levels indicate that human MSC engraftment and direct involvement in the regeneration of the BM via replenishment of damaged cells are unlikely explanations for our previous observations. The finding that injected D^{hi} MSCs can reverse BM damage despite not engrafting within the marrow is consistent with other studies documenting the therapeutic mechanisms of (unsorted) MSCs in similar injury models [1, 3, 6].

D^{hi} MSCs Function More Potently as Cell Factories Than Do D^{lo} MSCs to Mediate BM Recovery

An increasing volume of experimental evidence indicates that MSC-derived regenerative effects are mediated primarily via secreted factors [1, 3]. We therefore examined whether the efficacy observed with whole-cell infusions could be reproduced with secreted factors from MSCs. An identical quantity of size-sorted MSCs that was administered in an injected cell dose (20×10^6 cells per kg) was used to produce a concentrated secretome in serum-free medium. That MSC secretome was then administered in four intravenous injections to irradiated mice once every 48 hours after lethal irradiation. Although injections of D^{hi} MSC

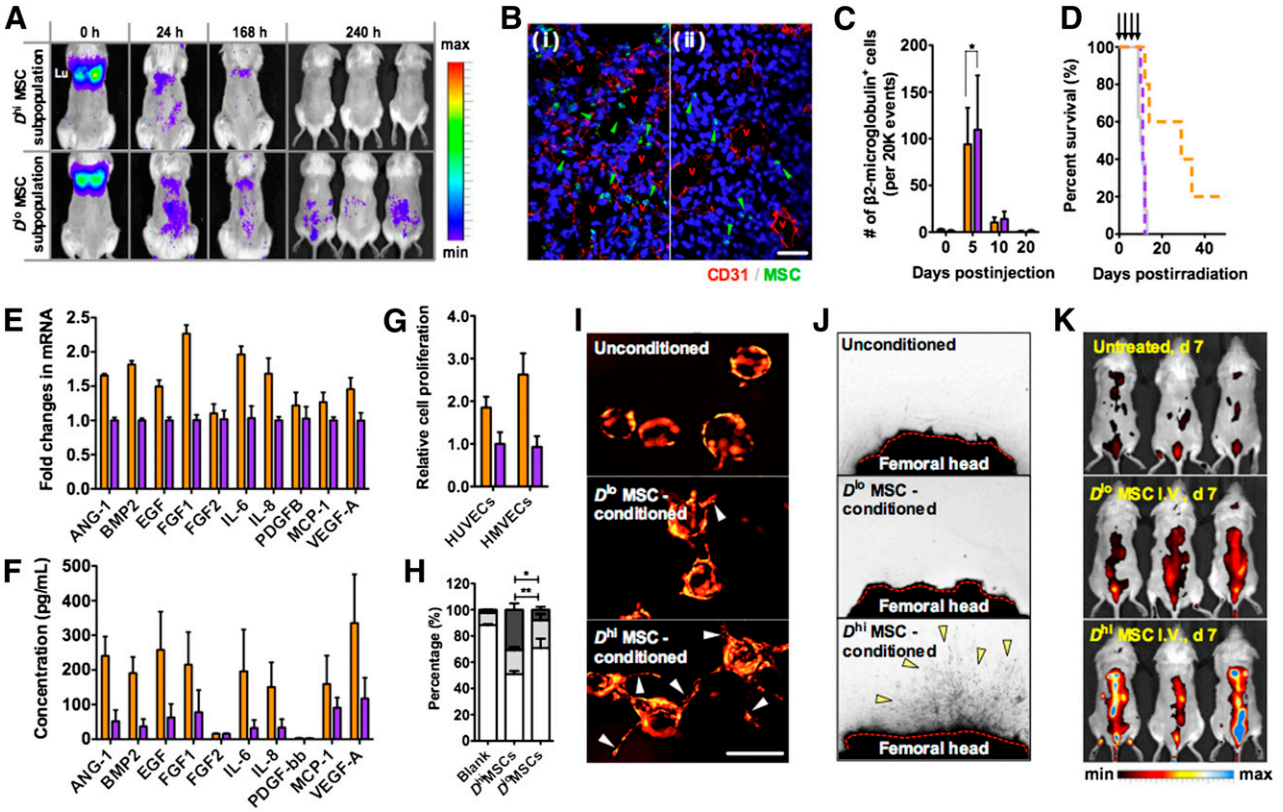

Figure 5. D^{hi} MSCs mediate tissue repair via secreted factors. **(A):** Dorsal view of the in vivo biodistribution of systemically injected luciferase transformed MSCs in sublethally irradiated NOD/SCID mice (2.5 Gy) over a period of 10 days. MSCs of both D^{hi} and D^{lo} MSC subpopulations initially accumulate in the lungs but redistribute over a 24-hour period. **(B):** No significant engraftment or extravasation of MSCs was found in the lungs after 24 hours, with most of the remaining MSCs localized within the capillary lumen in the lung tissue (**[Bi]** vs. **[Bii]**). After cell redistribution from the lungs, MSCs of both subpopulations also did not show any specific accumulation to the bone marrow (BM) or any other tissue and are significantly cleared from the body after 10 days. Scale bar = 100 μm. **(C):** Fluorescence-activated cell sorting analysis of femoral BM aspirates at different time points after MSC injection showed an insignificant degree of homing of injected MSCs to the BM. On day 5, ~0.02% of the injected MSC dose (for both D^{hi} and D^{lo} MSC subpopulations) was detected in the femoral BM, and no MSCs were detected by day 20. $n > 4$ femoral BM aspirates, 20,000 events analyzed. *, $p = .9626$. **(D):** Survival of lethally irradiated NOD/SCIDs ($n > 5$ mice) given regular injections (indicated by arrows) of secretome from the different MSC subpopulations. The median survival times were 29 and 11 days for the D^{hi} MSC and D^{lo} MSC secretome therapy groups, respectively. **(E, F):** D^{hi} versus D^{lo} MSC subpopulation reverse transcription-polymerase chain reaction and secretome analysis showed increased production (~3.8× on average) of soluble factors associated with angiogenesis, cell proliferation, and wound healing (IL-6, IL-8, EGF, FGF1, VEGF-A, Ang-1, etc.). Secretome from three MSC donors were tested in triplicate. **(G):** Relative proliferation rates of HUVECs and HMVECs after 48 hours of exposure to different MSC subpopulation secretome; cell proliferation was measured to be ~1.8× and ~2.5× higher when the D^{hi} MSC secretome was supplied to HUVECs and HMVECs, respectively, as compared with the D^{lo} MSC secretome. Proliferation rates were normalized to the D^{lo} MSC group ($n = 4$ wells). **(H):** Cell cycle analysis of HUVECs and HMVECs after exposure to different conditioned medium for 48 hours. The white bars show the G_0 phase, the light gray bars show the G_1 phase, and the dark gray bars show the G_2/S/M phase. *, $p = .022$ for the G_0 phase; **, $p = .0098$ for the G_2/S/M phase. **(I):** In vitro three-dimensional angiogenic sprouting assay of mCherry-transduced HUVECs in a fibrin gel (2.5 mg/ml) supplemented with different MSC secretomes. Arrows indicate position of angiogenic sprouts from HUVEC-loaded microcarrier beads. Scale bar = 100 μm. **(J):** Explanted femoral bones from lethally irradiated mice (5 days after) in a fibrin gel exposed to different MSC secretome. The red dotted line represents sectioned femoral head to expose the BM. After 10 days, capillary sprouts from the BM were observed in the D^{hi} MSC secretome-treated explants. **(K):** Blood vessel density in the BM of lethally irradiated NOD/SCIDs in **(D)** on day 7 visualized by angiosense (a near infrared in vivo imaging probe; dorsal view of mice). In comparison with the untreated group or D^{lo} secretome-treated group, the administration of D^{hi} MSC secretome led to increased angiogenesis in the BM. All values are given as means ± SD. The orange graphs show the D^{hi} MSC subpopulation, the purple graphs show the D^{lo} MSC subpopulation, and the dark gray graphs show the unsorted MSC population. All MSCs were used at passage 6. Abbreviations: Ang-1, angiopoietin-1; BMP2, bone morphogenetic protein 2; d, day; EGF, epidermal growth factor; FGF1, fibroblast growth factor 1; FGF2, fibroblast growth factor 2; h, hour(s); HMVEC, human microvascular endothelial cell; HUVEC, human umbilical vein endothelial cell; IL-6, interleukin-6; IL-8, interleukin-8; max, maximum; MCP-1, monocyte chemotactic protein 1; min, minimum; MSC, mesenchymal stromal cell; PDGFB, platelet-derived growth factor B; VEGF-A, vascular endothelial growth factor A.

secretome did not fully recapitulate the results observed with whole cell injections, they imparted a significant survival benefit compared with untreated mice. In contrast, effects of injected secretome from D^{lo} MSCs were negligible (Fig. 5D). The median survival times for the secretome therapy groups were 29 and 11 days, respectively, as compared with >50 and 13 days for the corresponding cell injections.

We next examined possible differences in the expression of growth factors and cytokines that could account for our observations. Both transcript and secreted protein levels of known regenerative factors [3, 5] such as interleukin-6 (IL-6), interleukin-8 (IL-8), vascular endothelial growth factor A (VEGF-A), bone morphogenetic protein 2, epidermal growth factor (EGF), fibroblast growth factor 1 (FGF1), and angiopoietin-1 were upregulated in

the D^{hi} MSC subpopulation (Figs. 5E, 5F). Additional data for other analyzed proteins, as well as comparisons of the secretome for unsorted MSCs at different passages, are shown in supplemental online Figure 9A and 9B. Despite the increased prevalence of D^{hi} MSCs in later passages (after P8–P9), we found that the quantity of protein secreted in later MSC passages decreased. β-Galactosidase staining indicated that a significant fraction of the subpopulation was senescent by P8–P9 (~20–25 population doublings). This increased number of D^{hi} MSCs that are senescent at elevated passages could negatively affect the capacity for D^{hi} MSCs to function as cell factories that produce sustained levels of therapeutic factors (supplemental online Fig. 10).

Because endothelial cell proliferation and angiogenesis were observed during in vivo BM recovery, we investigated the contribution of the MSC subpopulation secretomes toward these processes. Human umbilical vein endothelial cells (HUVECs) and human microvascular endothelial cells (HMVECs) cultured in the presence of D^{hi} MSC secretome proliferated at higher rates than those cultured in D^{lo} MSC secretome (1.8× and 2.5× greater for D^{hi} MSC secretome added to HUVECs and HMVECs, respectively; Fig. 5G). The cell cycle distribution of HUVECs was approximately 50% in the G_0 phase, 18% in the G_1 phase, and 32% in the G_2/M phase, 48 hours after introduction of the D^{hi} MSC secretome; however, this distribution remained predominantly in the G_0 and G_1 phases (>70% and >25%, respectively) with the D^{lo} MSC secretome or unconditioned medium (Fig. 5H). Endothelial sprout formation in vitro was also enhanced in the presence of the D^{hi} MSC secretome (Fig. 5I), but not by introduction of the D^{lo} MSC secretome or unconditioned medium. Finally, a proangiogenic effect was also observed with the use of D^{hi} MSC secretome on explanted irradiated (3.5 Gy) femur bone tissue. After 5–10 days of incubation with the D^{hi} MSC secretome, endothelial sprouts emanated from the severed ends of femoral head explants, whereas such extent of sprouting was not observed in the other treatment groups (Fig. 5J). In vivo, the secretome from the D^{hi} MSCs also led to the greatest degree of angiogenesis in the BM of lethally irradiated mice, as evidenced by whole body imaging using a fluorescent angiogenic probe (Fig. 5K). Whereas untreated mice exhibited barely detectable levels of the angiogenic probe, the spinal column of mice given MSC secretome showed fluorescent probe accumulation. The highest accumulation levels, indicative of greatest angiogenic activity, occurred in D^{hi} MSC secretome treatment groups.

Discussion

A central challenge to translational use of culture-expanded MSCs remains the consistent and high levels of therapeutic efficacy of cells obtained from readily available sources. Subtle differences in donor, source, culture methods, and expansion levels can affect cell population heterogeneity and functional outcomes. To realize the potential of MSC-based therapies, the variable efficacies of the final culture-expanded product must be addressed. Heuristic failure analyses of MSC clinical trials involving large patient groups suggest that even when the consistency of MSC biology was maintained with similar MSC-harvesting procedures, the process of culture expansion can introduce artifacts that can greatly affect the therapeutic quality of the expanded cell population [9, 32]. Because MSCs inherently exhibit functional plasticity, conditions that promote extensive in vitro proliferation to achieve a sufficiently large cell quantity for clinical or industrial use also tend to exert selection pressures that foster clonal impoverishment, lineage commitment, and a resultant biology that differs significantly from not only the initial MSC population, but also among culture-expanded populations of differing passage from a given donor source [9]. Thus, a heterogeneous mixture of MSCs is produced when larger cell numbers are required for translation, obfuscating realization of consistent therapy.

Here, we devised a cell sorting strategy for culture-expanded MSCs that can homogenize the therapeutic properties and deliver consistency in translational applications. Through new understanding of the mechanisms governing MSC-induced tissue regeneration, we hypothesized and experimentally verified that the larger or D^{hi} MSCs are an osteoprogenitor-enriched subpopulation defined by restricted differentiation in vitro (Fig. 2C, 2F) and also provide paracrine signaling to stimulate endogenous tissue recovery in vivo. The regenerative secretome of this MSC subpopulation provides relevant growth factors and cytokines after systemic administration, including proangiogenic factors (Fig. 5E, 5F; supplemental online Fig. 9). This paracrine mechanism is supported by our observations of a remarkable increase in survival of lethally irradiated mice after systemic infusion of D^{hi} MSCs (Fig. 3), but no detectable D^{hi} MSC engraftment or differentiation into new tissue within the lethally irradiated bone marrow (Fig. 5C; supplemental online Fig. 8).

The potential for ostoprogenitors to promote such repair has been alluded to by others, for example when BM MSCs were found to transiently increase in osteogenic activity, as well as osteogenic gene expression, during the recovery period from radiation damage [19–22]. However, this finding has yet to be translated into a viable form of therapy. Such delayed realization is due in part to the impracticality of extracting osteoprogenitors/osteoblasts from BM and to a general dearth of studies examining MSC subpopulation properties in expanded cultures that may enable new discoveries and uses. Label-free biophysical cell sorting also facilitates realization of this approach without the need for traditional antibody or other biochemical modifications that are associated with technical and regulatory complexities. Although other label-free methods to enrich cell subpopulations on the basis of cell size exist (e.g., physical filtration or flow cytometry), the present demonstration via inertial microfluidics confers concurrent advantages of low cost, high throughput, and high cell viability postsorting.

Compared with other treatment groups, systemic administration of the osteoprogenitor-enriched D^{hi} MSC subpopulation resulted in enhanced regeneration of BM tissue and increased survival times after irradiative damage. There was no evidence of long-term MSC engraftment within the BM tissue, and further experiments demonstrated that regular injections of conditioned medium from this subpopulation partially reproduced the effect of cell injections. These observations, together with data showing the increased capacity of D^{hi} MSCs to secrete regenerative factors, are consistent with other studies documenting MSC-mediated therapeutic mechanisms via apparent paracrine signaling. Further, our findings in vitro and in vivo support the concept that D^{hi} MSCs function primarily as cell factories after systemic injection to mediate tissue repair via nonosteogenic lineages that enhance revascularization (Fig. 4F, 4G). The multitude of beneficial factors secreted by D^{hi} MSCs has the potential to modulate the injured cellular milieu on multiple fronts, thus evoking sustained and enhanced tissue regeneration including angiogenesis (Fig. 5J). This ability for a systems approach to tissue repair has

been demonstrated extensively to be critically important in applications for tissue regeneration using drug- or biologic-eluting biomaterials [33, 34]. D^{hi} MSCs thus represent a natural systems-based therapy for tissue repair across immunological barriers; current clinical data support the long-term safety profile of systematically delivered MSC therapy for the treatment of various diseases: dosages as high as 10^8 MSCs/kg from nonrelated donors have been administered without long-term complications [35–37]. This tolerance generates a high level of enthusiasm within the scientific and medical communities for the continued development of adult MSC-based therapies. Furthermore, the demonstrated safety profile of adult MSCs from unrelated donors paves the way for the use of culture-expanded, biophysically sorted, and cryopreserved MSCs from a larger donor pool; such a bank would greatly facilitate the adoption of this cell-based tissue regenerative therapy.

Conclusion

The capacity of intravenously administered D^{hi} MSCs to support BM regeneration, including the revascularization and regeneration of essential hematopoiesis-supporting environments, could be used in hematopoietic stem cell transplant (HSCT) applications. BM vasculature is largely devoid of pericytes, and the surrounding stroma is the chief cellular moiety that provides architectural support and the capabilities for angiogenic remodeling to the BM vasculature [38]. This relationship makes the BM vasculature particularly vulnerable to myelosuppressive therapies that are intended to target cycling hematopoietic cells in the stroma, because the loss of their structural support further induces regression of BM sinusoids and necrosis of associated perivascular cells, including the essential HSC niches [19]. Hence, administration of D^{hi} MSCs as adjuvant therapy could foster a BM environment conducive to HSC homing and engraftment during HSCT. This translation could be particularly impactful for umbilical cord blood grafts, which are known to exhibit delayed engraftment kinetics that adds to the risk of the procedure [39]. Further, whereas the possibility of injury to BM vasculature and tissue through the use of radiation or certain chemotherapeutic agents is well established, this form of impairment of the hematopoiesis-supporting stroma has only recently been verified clinically to be associated with the development of poor graft function after HSC transplantation. Patients that develop poor hematopoietic graft function show marked BM hypocellularity with few detected microvessels and, importantly, significantly lower frequencies of HSC niche cells [40]. Here, D^{hi} MSC subpopulations can also be considered as treatment to improve hematopoietic function through regeneration of the BM stroma. In summary, biophysically sorted subpopulations of MSC-derived osteoprogenitors provide clear practical and therapeutic advantages for clinical translation, including applications in BM repair and hematopoiesis.

Acknowledgments

This work was supported by the National Research Foundation of Singapore through the BioSystems and Micromechanics Interdisciplinary Research Group and a Innovation Centre Ignition Grant of the Singapore-MIT Alliance for Research and Technology.

Author Contributions

Z.P.: conception and design, collection of data, data analysis and interpretation, manuscript writing; W.C.L. and G.G.: provision of study material, collection of data, data analysis and interpretation; L.M.N.: provision of study material, data analysis and interpretation; C.T.L. and J.H.: final approval of manuscript, data analysis and interpretation; K.J.V.V.: conception and design, data analysis and interpretation, manuscript writing, financial support, final approval of manuscript.

Disclosure of Potential Conflicts of Interest

J.H. has uncompensated intellectual property rights in a patent describing the technology used in the paper that was filed and assigned to the Massachusetts Institute of Technology. The other authors indicated no potential conflicts of interest.

References

1 Keating A. Mesenchymal stromal cells: New directions. Cell Stem Cell 2012;10:709–716.

2 Horwitz EM. MSC: A coming of age in regenerative medicine. Cytotherapy 2006;8:194–195.

3 Ranganath SH, Levy O, Inamdar MS et al. Harnessing the mesenchymal stem cell secretome for the treatment of cardiovascular disease. Cell Stem Cell 2012;10:244–258.

4 Horwitz EM, Dominici M. How do mesenchymal stromal cells exert their therapeutic benefit? Cytotherapy 2008;10:771–774.

5 Heo SC, Jeon ES, Lee IH et al. Tumor necrosis factor-α-activated human adipose tissue-derived mesenchymal stem cells accelerate cutaneous wound healing through paracrine mechanisms. J Invest Dermatol 2011;131:1559–1567.

6 Yang X, Balakrishnan I, Torok-Storb B et al. Marrow stromal cell infusion rescues hematopoiesis in lethally irradiated mice despite rapid clearance after infusion. Adv Hematol 2012;2012:142530.

7 Sorrell JM, Caplan AI. Topical delivery of mesenchymal stem cells and their function in wounds. Stem Cell Res Ther 2010;1:30.

8 Bianco P, Riminucci M, Gronthos S et al. Bone marrow stromal stem cells: Nature, biology, and potential applications. Stem Cells 2001;19:180–192.

9 Phinney DG. Functional heterogeneity of mesenchymal stem cells: Implications for cell therapy. J Cell Biochem 2012;113:2806–2812.

10 Morad V, Pevsner-Fischer M, Barnees S et al. The myelopoietic supportive capacity of mesenchymal stromal cells is uncoupled from multipotency and is influenced by lineage determination and interference with glycosylation. Stem Cells 2008;26:2275–2286.

11 Al-Nbaheen M, Vishnubalaji R, Ali D et al. Human stromal (mesenchymal) stem cells from bone marrow, adipose tissue and skin exhibit differences in molecular phenotype and differentiation potential. Stem Cell Rev 2013;9:32–43.

12 Lee RH, Kim B, Choi I et al. Characterization and expression analysis of mesenchymal stem cells from human bone marrow and adipose tissue. Cell Physiol Biochem 2004;14:311–324.

13 Ehninger A, Trumpp A. The bone marrow stem cell niche grows up: Mesenchymal stem cells and macrophages move in. J Exp Med 2011;208:421–428.

14 El-Badri NS, Wang BY, Cherry et al. Osteoblasts promote engraftment of allogeneic hematopoietic stem cells. Exp Hematol 1998;26:110–116.

15 Greenbaum A, Hsu YM, Day RB et al. CXCL12 in early mesenchymal progenitors is required for haematopoietic stem-cell maintenance. Nature 2013;495:227–230.

16 Ding L, Morrison SJ. Haematopoietic stem cells and early lymphoid progenitors occupy distinct bone marrow niches. Nature 2013;495:231–235.

17 Kopp HG, Hooper AT, Avecilla ST et al. Functional heterogeneity of the bone marrow vascular niche. Ann N Y Acad Sci 2009;1176:47–54.

18 Park D, Spencer JA, Koh BI et al. Endogenous bone marrow MSCs are dynamic, fate-restricted participants in bone maintenance and regeneration. Cell Stem Cell 2012;10:259–272.

19 Cao X, Wu X, Frassica D et al. Irradiation induces bone injury by damaging bone marrow

microenvironment for stem cells. Proc Natl Acad Sci USA 2011;108:1609–1614.

20 Hooper AT, Butler JM, Nolan DJ et al. Engraftment and reconstitution of hematopoiesis is dependent on VEGFR2-mediated regeneration of sinusoidal endothelial cells. Cell Stem Cell 2009;4:263–274.

21 Shirota T, Tavassoli M. Cyclophosphamide-induced alterations of bone marrow endothelium: Implications in homing of marrow cells after transplantation. Exp Hematol 1991;19: 369–373.

22 Zeng L, Yan Z, Ding S et al. Endothelial injury, an intriguing effect of methotrexate and cyclophosphamide during hematopoietic stem cell transplantation in mice. Transplant Proc 2008;40:2670–2673.

23 Poncin G, Beaulieu A, Humblet C et al. Characterization of spontaneous bone marrow recovery after sublethal total body irradiation: Importance of the osteoblastic/adipocytic balance. PLoS ONE 2012;7:e30818.

24 Robey PG, Termine JD. Human bone cells in vitro. Calcif Tissue Int 1985;37:453–460.

25 Li Z, Liu C, Xie Z et al. Epigenetic dysregulation in mesenchymal stem cell aging and spontaneous differentiation. PLoS ONE 2011;6: e20526.

26 Boxall SA, Jones E. Markers for characterization of bone marrow multipotential stromal cells. Stem Cells Int 2012;2012:975871.

27 Kolf CM, Cho E, Tuan RS. Mesenchymal stromal cells: Biology of adult mesenchymal stem cells: Regulation of niche, self-renewal and differentiation. Arthritis Res Ther 2007;9:204.

28 Lee WC, Shi H, Poon Z et al. Needle in a haystack: Biophysical markers predictive of mesenchymal stromal cell multipotency. Proc Natl Acad Sci USA 2014;111:E4409–E4418.

29 Wu L, Guan G, Hou HW et al. Separation of leukocytes from blood using spiral channel with trapezoid cross-section. Anal Chem 2012; 84:9324–9331.

30 Guan G, Wu L, Bhagat AA et al. Spiral microchannel with rectangular and trapezoidal cross-sections for size based particle separation. Sci Rep 2013;3:1475.

31 Whitfield MJ, Lee WC, Van Vliet KJ. Onset of heterogeneity in culture-expanded bone marrow stromal cells. Stem Cell Res (Amst) 2013;11:1365–1377.

32 Galipeau J. The mesenchymal stromal cells dilemma: Does a negative phase III trial of random donor mesenchymal stromal cells in steroid-resistant graft-versus-host disease represent a death knell or a bump in the road? Cytotherapy 2013;15:2–8.

33 Chen FM, Zhang M, Wu ZF. Toward delivery of multiple growth factors in tissue engineering. Biomaterials 2010;31:6279–6308.

34 Park JS, Yang HN, Woo DG et al. The promotion of chondrogenesis, osteogenesis, and adipogenesis of human mesenchymal stem cells by multiple growth factors incorporated into nanosphere-coated microspheres. Biomaterials 2011;32:28–38.

35 Jung S, Panchalingam KM, Wuerth RD et al. Large-scale production of human mesenchymal stem cells for clinical applications. Biotechnol Appl Biochem 2012;59:106–120.

36 Schallmoser K, Rohde E, Reinisch A et al. Rapid large-scale expansion of functional mesenchymal stem cells from unmanipulated bone marrow without animal serum. Tissue Eng Part C Methods 2008;14:185–196.

37 Kean TJ, Lin P, Caplan AI et al. MSCs: Delivery routes and engraftment, cell-targeting strategies, and immune modulation. Stem Cells Int 2013;2013:732742.

38 Kopp HG, Avecilla ST, Hooper AT et al. The bone marrow vascular niche: Home of HSC differentiation and mobilization. Physiology (Bethesda) 2005;20:349–356.

39 Ballen KK, Gluckman E, Broxmeyer HE. Umbilical cord blood transplantation: The first 25 years and beyond. Blood 2013;122:491–498.

40 Kong Y, Chang YJ, Wang YZ et al. Association of an impaired bone marrow microenvironment with secondary poor graft function after allogeneic hematopoietic stem cell transplantation. Biol Blood Marrow Transplant 2013; 19:1465–1473.

See www.StemCellsTM.com for supporting information available online.

